Scaling Relations and Size Control of Block Ionomer Microreactors Containing Different Metal Ions

Matthew Moffitt and Adi Eisenberg*

Department of Chemistry, McGill University, 801 Sherbrooke Street West, Montreal, P.Q., Canada H3A 2K6

Received October 23, 1996; Revised Manuscript Received March 25, 1997[⊗]

ABSTRACT: Block ionomer micelles of polystyrene-*b*-poly(metal acrylate) containing a wide range of metal ions have been characterized, in order to establish a priori size control for a system of inorganic microreactors in which metal ions can be converted via simple chemistry to metallic or semiconducting nanoparticles. A variety of techniques have been employed, including size-exclusion chromatography (SEC), static light scattering (SLS), dynamic light scattering (DLS), and transmission electron microscopy (TEM). Scaling relations for aggregation numbers (Z) and ionic core radii (R_{core}) as a function of the ionic block length (N_B) have been determined: $Z \sim N_B^{0.74\pm0.08}$; $R_{core} \sim N_B^{0.58\pm0.03}$, where the proportionality constants $K_{Z,ave}$ and $K_{R,ave}$ are dependent on the metal ion and decrease as $Ni^{2+} > Cs^{+} > Co^{2+} > Ba^{2+} > Cd^{2+} > Pb^{2+}$. For most metal ions, linear plots of R_{core} vs $N_B^{0.58}$ yield correlation coefficients of r^2 of ca. 0.99, indicating excellent size control of ionic core radii. We also find that $K_{Z,ave}$ decreases linearly with the crystal ionic radius (r_{ion}) for block ionomers neutralized with metal acetates. We speculate upon the role of the metal ion on micelle growth. Comprehensive scaling laws have also been determined to include the soluble block length dependence, and similar exponents were found for most metal ions. DLS results show R_g/R_h values between those of stars and compact spheres. The coronal brush height (H) is found to scale as $H \sim Z^{0.3\pm0.1}N_A^{0.9\pm0.2}$, in reasonable agreement with the Daoud and Cotton model for starlike systems.

1. Introduction

It has been known for some time that block copolymers tend to self-assemble in selective solvents, forming aggregates that are structurally analogous to micelles of associated surfactant molecules.[1−3] The driving force for micellization is generally attributed to microphase precipitation of the insoluble blocks, although the final structure of the micelle is an expression of both enthalpic and entropic factors. When there are relatively small differences between the polymer−solvent interaction parameters of the two blocks (χ_{AS}, χ_{BS}), the micelles exist in the weak segregation limit, with low interfacial tension between the micelle core and the surrounding solvent.

More recently, an increasing amount of attention has focused on the micellization of ionic diblock copolymers, which consist of an ionic block covalently linked to a nonionic block.[4−6] These materials can be classified as polymeric amphiphiles, with large solubility differences between hydrophilic and hydrophobic moieties. Two types of ionic diblock copolymer micelles can be distinguished, depending on the nature of the selective solvent. In aqueous media, ionic diblock copolymers exist as block polyelectrolyte micelles, sometimes referred to as "regular micelles", with hydrophobic cores solubilized by ionic coronas. In organic media, the insolubility of the hydrophilic ionic blocks results in block ionomer (or "reverse") micelles. Compared with their nonionic counterparts, both classes of ionic diblock copolymers are characterized by extremely low critical micelle concentrations (cmc's), indicative of strong driving forces for micellization. The interfacial tension between the cores and the solvent (and between ionic and nonionic blocks) is relatively high, and the micelles exist in the strong or perhaps even superstrong segregation limit.

The present study is concerned with the characterization of diblock ionomer micelles in organic solvents, specifically micelles of polystyrene-*b*-poly(metal acrylate) ionomers. These aggregates generally consist of block copolymers in which the number of insoluble ionic repeat units (N_B) is very small compared with the number of soluble styrene repeat units ($N_B << N_A$) and fall into the category of "starlike" micelles due to their small, compact cores and large, extended coronas. Our interest in these materials has been spurred by the potential applications of poly(metal acrylate) ionic cores as inorganic microreactors of controllable size, in which various metal counterions can be converted via simple chemistry to metallic or semiconducting nanoparticles. The size of the inorganic particles growing in such microreactors will be determined by the aggregation number of the block ionomer; after chemical conversion, the core regions will then protect the particles dispersed in the matrix phase from growth mechanisms such as agglomeration and Ostwald ripening.

In a previous publication, we described the synthesis of CdS nanoparticles within reverse micelles of polystyrene-*b*-poly(cadmium acrylate) (PS-*b*-PACd) by reaction of the ionic cores with hydrogen sulfide (H_2S).[7] The particle sizes showed excellent correlation with the sizes of the original ionic cores, demonstrating that a priori size control of CdS particles is possible. The CdS−polymer composites were reneutralized with NaOH to increase the micelle stability, after which the materials could be repeatedly dissolved in organic solvents and precipitated into methanol, or compression-molded above 100 °C, without the observation of Ostwald ripening or particle agglomeration. The CdS nanoparticles were found to be relatively monodisperse, with radius polydispersity indices (RPI) of ca. 1.04. Controlled secondary growth of CdS nanoparticles within the micelle cores was also demonstrated, by "reloading" the PAA blocks with cadmium acetate, followed by secondary reaction with H_2S.

* To whom all correspondence should be addressed.
[⊗] Abstract published in *Advance ACS Abstracts,* July 1, 1997.

S0024-9297(96)01577-X CCC: $14.00 © 1997 American Chemical Society

Other groups have also employed ion-containing polymers in the synthesis of nanoparticles,[8−12] although clear correlations between the composition of the polymer host and the size of the particles are still rare. In most polymer systems, the strategy for nanoparticle synthesis involves the formation of micelles with metal-complexing insoluble blocks, followed by the incorporation of metal ions into the cores and their subsequent conversion to metals or semiconductors. Block copolymers with such core-forming blocks as poly(2-vinylpyridine),[8] norbornene-based polymers,[9,10] poly(4-vinylpyridine),[11] and poly(ethylene oxide)[12] have all been applied to synthesize a wide range of metallic and semiconducting nanoparticles.

In the present work, our preparation of microreactors employs a different approach to the incorporation of metal ions into the micelle cores. To form reverse micelles of polystyrene-*b*-poly(metal acrylate) ionomers, single chains of polystyrene-*b*-poly(acrylic acid) (PS-*b*-PAA) are neutralized with various metal ions, which induces self-assembly of insoluble ionic blocks. In contrast to the methods employed in refs 8−12, the metal ions not only are inorganic "guests" but also act as counterions for the neutralized PAA blocks. Also, by the present method, micellization and the incorporation of ions into the micelle core do not occur in separate steps; rather, these are simultaneous and mutually dependent processes arising from the neutralization of acid units. Along with the inherent stability of the micelles, we believe that the present strategy offers several advantages over other systems, such as (1) the controlled introduction of metal ions by acid−base titration, (2) the effective localization of ions within the micelle core, and (3) the wide range of complexing and noncomplexing metals that can be incorporated into the core. It is important to note that, since micellization is initiated by the neutralization of the acid block, the effect of the nature of the counterion on self-assembly must be considered and is of fundamental importance to our quest for a priori size control.

From the point of view of material science, the control of nanoparticle sizes within a polymer matrix is of great interest, as a means of producing composites with specific electronic and optical properties. These properties are largely determined by the sizes of metallic or semiconducting nanoparticles within the matrix, through various quantum-confinement and surface effects.[13,14] Thus, if nanoparticle sizes are controlled by the composition of the matrix, a situation arises in which the properties of a polymer/inorganic composite are easily "tuned" through the selection of an appropriate polymer host. The control of block copolymer composition can be achieved by well-established techniques of sequential anionic polymerization. However, in order to establish relationships between the composition of the block copolymer and the ultimate sizes of the guest nanoparticles, two conditions must be met. First, a priori knowledge of micelle aggregation numbers as a function of soluble and insoluble block lengths should be obtained for the system of interest. Second, the complete conversion of ions to a single particle in each core should be achieved, such that the size of the particles and the micelle aggregation number are closely correlated. Single particles in the cores of block copolymer micelles are described in the literature and are generally formed by heating[10,12] or placticizing[7] the ion-containing microdomains. In the field of material science, however, little attention has been given to the first of these conditions.

Table 1. Molecular Characteristics of Polystyrene-*b*-poly(acrylic acid) Copolymers

PS(*x*)-*b*-PAA(*y*)	mol %PAA	M_n	PI
370-*b*-3	0.8	38 800	1.04
370-*b*-7	1.9	39 000	1.04
370-*b*-11	2.9	39 300	1.04
370-*b*-15	3.9	39 600	1.04
370-*b*-19	4.9	39 900	1.04
370-*b*-26	6.6	40 400	1.06
730-*b*-84	10.3	82 100	1.08
300-*b*-44	12.8	34 600	1.05

This work continues earlier investigations of polystyrene-*b*-poly(methacrylic acid) (PS-*b*-PMAA) and PS-*b*-PAA-based block ionomers, in which cesium and sodium were the counterions of the neutralized acid block.[15−17] In these systems, gel-permeation chromatography, viscometry, dynamic and static light scattering, transmission electron microscopy, and small-angle X-ray scattering were used to probe micelle aggregation numbers and ionic core sizes as a function of block lengths. Here we look at a wider range of counterions from across the periodic table, in order to establish scaling relationships between block copolymer composition and micelle aggregation numbers for a variety of potential inorganic microreactors. We also demontrate simple chemistry within one type of microreactor, through the production of Pb^0 particles in the cores of Pb^{2+} block ionomer micelles. Along with such applications to material science, this investigation is also of interest on a more fundamental level, as it is the first detailed study of block ionomer micellization as a function of counterion.

2. Experimental Section

2.1. Synthesis of PS-*b*-PAA Diblock Copolymers. The diblock copolymers used in the present study (Table 1) were synthesized by known procedures;[15,18,19] therefore, only a brief summary is presented here. In the table, $x = N_A$, and $y = N_B$.

Sequential anionic polymerization was used to prepare series of polystyrene-*b*-poly(*tert*-butyl acrylate) (PS-*b*-PtbA) with polystyrene blocks of constant length and poly(*tert*-butyl acrylate) blocks of variable length. In this procedure, the styrene monomer is polymerized first; then a precise amount of the second monomer is added to the solution of "living" polymer chains. A sample of block copolymer is extracted from the flask, followed by the next addition of the second monomer. Thus, six samples of diblock copolymers with identical polystyrene blocks of 370 units and six different PtbA block lengths, ranging from 3 to 26 repeat units, were prepared in a single synthetic run. The other two diblock copolymers used in this study, PS(300)-*b*-PtbA(44) and PS(730)-*b*-PtbA(84), were individual samples from two independent series.

For all series of diblock copolymers, anionic polymerization in tetrahydrofuran (THF) was initiated by *sec*-butyllithium capped with a few units of α-methylstyrene. The molecular weights of the polystyrene blocks, and the polydispersity indexes of each block copolymer (PI), were determined by size-exclusion chromatography (SEC) in THF. As shown in Table 1, all block copolymers used in the present study had polydispersity indexes between 1.04 and 1.08. The lengths of the *tert*-butyl acrylate blocks were determined by quantitative Fourier-transform infrared spectroscopy (FTIR) of samples dissolved in carbon tetrachloride. Block copolymers in the ester form were then hydrolyzed, by refluxing overnight in toluene with small amounts of *p*-toluenesulfonic acid catalyst. The polymers in the acid form were precipitated into methanol and then dried in a vacuum oven at 70 °C for at least 24 h. A few samples showed incomplete hydrolysis, and these were subsequently hydrolyzed to completion by dissolving the polymers in an 80/20 mixture of toluene/acetic acid (v/v) and refluxing for 2 h with methanesulfonic acid catalyst.[20]

2.2. Preparation of Block Ionomer Micelles. Block copolymers in the acid form were dissolved in benzene/methanol (10% methanol v/v) to obtain solutions of 2% polymer (w/w). To form micelles containing Cs^+, Ba^{2+}, Cd^{2+}, Pb^{2+}, Ni^{2+}, and Co^{2+}, single chains of PS-*b*-PAA were neutralized by the addition of methanolic solutions (0.10 or 0.25 M) of cesium hydroxide monohydrate ($Cs(OH)\cdot H_2O$), barium hydroxide octahydrate ($Ba(OH)_2\cdot 8H_2O$), cadmium acetate dihydrate ($Cd(Ac)_2\cdot 2H_2O$), lead acetate trihydrate ($Pb(Ac)_2\cdot 3H_2O$), nickel acetate tetrahydrate ($Ni(Ac)_2\cdot 4H_2O$), and cobalt acetate tetrahydrate ($Co(Ac)_2\cdot 4H_2O$), respectively.

For the neutralization of PS-*b*-PAA with $Cs(OH)\cdot H_2O$, a stoichiometric quantity of neutralizing agent was added. Neutralizing agents with divalent cations were added in excess (R = moles of neutralizing reagent/moles of acrylic acid repeat units), such that $R = 1.5$. It should be noted that, in the case of divalent counterions, this represents an excess of 3 equiv (i.e., moles of acetate or hydroxide ions) per mole of acrylic acid units.

After addition of the neutralizing agent, all solutions were stirred for at least 1 h. Neutralized block ionomers (reverse micelles) were recovered by freeze-drying and then dried under vacuum at 70 °C to remove the remaining solvent and acetic acid. Excess metal acetate or metal hydroxide was removed by repeated washings of the micelles in methanol, and the washed polymers were dried overnight under vacuum at 70 °C. FTIR spectra confirmed that the ionomers were 100% neutralized.

2.3. Size-Exclusion Chromatography of Block Ionomers. Size-exclusion chromatography (SEC) measurements of the reverse micelles were performed using a Varian Model 5000 liquid chromatograph equipped with a refractive index detector. The data were collected and analyzed on a Varian DS-604 computer with appropriate SEC software. After freeze-drying and washing of the neutralized samples, small amounts of block ionomer were dissolved in THF. These solutions were filtered through membrane filters with a nominal pore size of 0.45 μm and then diluted to a concentration of about 2 g/L before injection into the SEC columns. Chromatograms generally showed two peaks at high and low elution volumes, attributed to single chains and micelles, respectively. The weight percentage of micellized chains was calculated from the relative areas under the two peaks. The error on the values, determined from three repeat measurements, was typically ca. 1%.

2.4. Static Light Scattering. Static light scattering (SLS) experiments were performed on a Dawn-F multiangle laser photometer (Wyatt Technology) fitted with a He−Ne laser (632.8 nm). Data acquisition and Zimm plot processing utilized DawnF and Aurora (Wyatt) software, respectively. Stock solutions of block ionomers were prepared by dissolving the neutralized polymers in toluene. To eliminate dust from all samples, stock solutions were filtered twice through membrane filters with a nominal pore size of 0.45 μm, transferred to a dust-free scintillation vial, and then diluted with filtered solvent. After each set of five repeat measurements, the micelle solutions were diluted with a known quantity of filtered toluene and allowed to sit for 10 min. Measurements were obtained at five different concentrations, in the range of 2.0−0.1 mg/mL. The range of concentrations for each sample varied with the molecular weight of the reverse micelles and was selected such that reasonable scattered intensity was obtained without saturation of the detectors.

2.5. Dynamic Light Scattering. Dynamic light scattering (DLS) experiments were performed on a Brookhaven Instruments photon correlation spectrometer equipped with a BI-2030 digital correlator and a He−Ne laser (632.8 nm) from Spectra Physics. The angle of detection was varied between 50 and 145° using a goniometer apparatus. All measurements were made at 25 °C over a range of concentrations and detection angles. Five repeat measurements of Γ (s^{-1}) (the relaxation rate of the autocorrelation function, $g_1(\tau)$) were made at each angle and concentration, and average values were taken.

To ensure that DLS measurements were not affected by dust, all glassware was rinsed, first with filtered reagent-grade acetone and then with acetone condensed from the vapor. Stock solutions of selected block ionomers in toluene were prepared, and these were filtered through membrane filters with a nominal pore size of 0.45 μm. Successive dilutions of sample solutions were performed by the addition of known quantities of toluene, filtered through 0.20 μm membrane filters.

2.6. Transmission Electron Microscopy. Transmission electron microscopy (TEM) was performed on a Phillips EM410 instrument. Solid-state block ionomers were prepared by casting solutions of reverse micelles from THF, followed by the evaporation of solvent. The films were then microtomed to a thickness of ca. 800 Å and mounted on a copper grid. Of the ionomers prepared in the present study, those containing metal ions with the highest atomic numbers (Pb^{2+}, Cs^+, Ba^{2+}, and Cd^{2+}) were investigated by TEM, in order to obtain adequate contrast of ions within the polymer.

3. Results and Discussion

This section is divided into four parts. In section 3.1, we describe size-exclusion chromatography (SEC) and static light scattering (SLS) results, including the calculation of aggregation numbers and ionic core radii for a wide range of block ionomers. The determination of scaling relations for micellar parameters as a function of ionic and nonionic block lengths is then discussed in section 3.2. Scaling relations for block ionomers containing different metal ions are compared, and we speculate upon the role of the counterion in micellar growth. Section 3.3 pertains to dynamic light scattering (DLS) results; the hydrodynamic behavior of block ionomers is discussed, especially in connection with micellar structure. Finally, in section 3.4, we consider transmission electron micrographs (TEM) of selected block ionomers containing different metal ions, including one in which Pb^{2+} ions have been partially converted into metal particles.

3.1. SEC and SLS of Block Ionomers. 3.1.1. Basic SLS Theory. If colloidal particles are of sufficient size ($>\lambda/20$), they are found to scatter light according to the following relation:[21]

$$\frac{Kc}{R(\theta)} = \frac{1}{P(\theta)M_w} + 2A_2c \qquad (1)$$

where $R(\theta)$ is the Rayleigh ratio at the angle of measurement, $P(\theta)$ is the particle scattering function, M_w is the weight-average molecular weight of the particle, and A_2 is the second virial coefficient. The optical constant, K, is defined:

$$K = 4\pi^2(n\ \mathrm{d}n/\mathrm{d}c)^2/\lambda_0{}^4N_A \qquad (2)$$

where n is the refractive index of the particle, dn/dc is the specific refractive index increment at constant chemical potential, N_A is Avogadro's number, and λ_0 is the wavelength of scattered light in a vacuum.

For SLS of block copolymer micelles, dn/dc is a function of the refractive indexes of both blocks; Zimm plot analysis yields an apparent molecular weight, $M_{w,app}$, which must be adjusted according to the chemical heterogeneity of the block copolymer to determine a true molecular weight.[22,23] However, for block ionomer micelles of the type studied in the present work, it has been found that dn/dc is identical to that of polystyrene in the appropriate solvent, such that $M_{w,app}$ is close to the true value of M_w.[24] In eq 2, the specific refractive index increment for polystyrene in toluene, dn/dc = 0.11, was therefore used to calculate K for all reverse micelles

Scheme 1

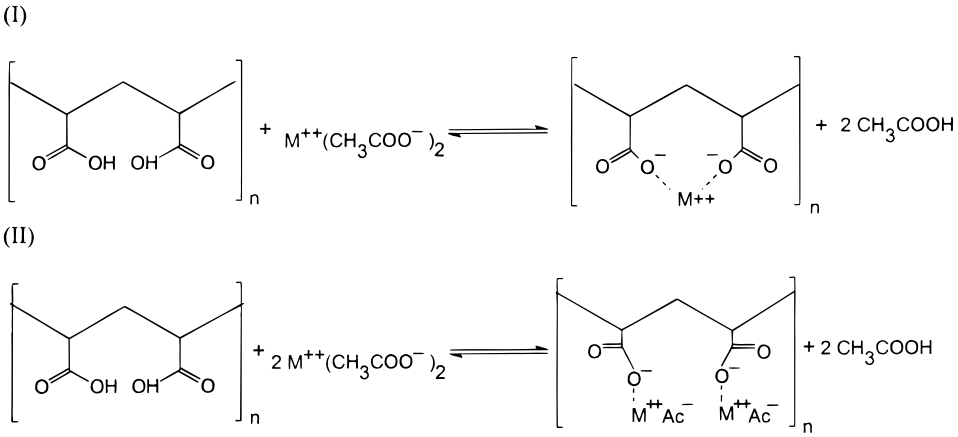

in this work. The low weight fraction of the ionic block and the compact nature of the small micelle core are both factors that make the chemical heterogeneity negligible in these materials.

3.1.2. SEC and SLS Results. The weight fraction of micelles, f_{mic}, was determined for each sample using SEC chromatography, from the relative areas of the micelle and single chain peaks. In block ionomers, which do not exhibit significant dissociation−association equilibria on a reasonable time scale, the single chain fraction is attributed to a mixture of homopolymer and diblocks with ionic segments that are too short to self-assemble.[15] For the shortest ionic blocks ($y = 3$ repeat units), f_{mic} values were found to be lowest in the Cd^{2+} ($f_{mic} = 0.04$) and Pb^{2+} ($f_{mic} = 0.08$) ionomers, indicating higher single-chain solubility and weaker ionic interactions for these two counterions. Ionomers neutralized with Cs^+ exhibit an intermediate micelle fraction for the shortest ionic block ($f_{mic} = 0.13$), while Ba^{2+}, Ni^{2+}, and Co^{2+} ionomers show the lowest solubility ($f_{mic} = 0.37 \pm 0.02$). For all counterions, single-chain solubility was found to decrease dramatically when $y > 3$, as evinced by a marked increase in f_{mic}.

From Zimm plot analysis,[21] the total molecular weights of block ionomers in toluene, $M_{w,tot}$, were determined. Since there are both single chain and micellar fractions present in solution, $M_{w,tot}$ is a weighted average of these two components:

$$M_{w,tot} = f_{mic}M_{w,mic} + f_{sc}M_{w,sc} \qquad (3)$$

where f_{mic} and $M_{w,mic}$ are the weight fraction and molecular weight of micelles in solution and f_{sc} and $M_{w,sc}$ are the weight fraction and molecular weight of the single chains.

With values of f_{mic} determined from SEC, and $M_{w,tot}$ from SLS measurements, the micellar molecular weights, $M_{w,mic}$, were calculated using eq 3. The average molecular weight of the single chain fraction, $M_{w,sc}$, was assumed to be equal to that of the polystyrene block. A complete list of f_{mic}, $M_{w,tot}$, and $M_{w,mic}$ values is included in the Supporting Information.

Aggregation numbers were calculated for each value of $M_{w,mic}$, using the molecular weight of unimers making up the micelle. In general, the molecular weights of micellized single chains depend on the final chemical state of the insoluble block, i.e., the percentage of "bridged" counterions in the micelle core. In the case of neutralization with metal acetates, two mechanisms of counterion binding are possible (Scheme 1).

Table 2. Aggregation Numbers of Block Ionomer Micelles Containing Different Metal Ions

polymer composition PS(*x*)-*b*-PAA(*y*)	type of metal ion					
	Cs^+	Ba^{2+}	Cd^{2+}	Pb^{2+}	Ni^{2+}	Co^{2+}
370-*b*-3	127	58	140	80	25	18
370-*b*-7	43	38	33	21	33	31
370-*b*-11	58	47	56	41	63	39
370-*b*-15	80	52	44	36	74	63
370-*b*-19	88	69	54		105	95
370-*b*-26	100	104	98	56	113	115
730-*b*-84	177	167	145	123	207	285
300-*b*-44	230	490	340	159	360	950

For any PAA block neutralized with metal acetate, a mixture of I and II is the most probable state,[7] though for the purpose of comparison we generally assume that one of these two equilibria is dominant. In the cases of Ba^{2+} and Cs^+, which were introduced in the form of metal hydroxides, these chemical equilibria are not operative, and all counterions are either bridged or unbridged, depending on the ionic valence.

It should be noted that, since the ionic content in these block ionomers is very low, the molecular weight of single chains is only weakly dependent on the extent of counterion bridging. Even for samples with the highest ionic content, aggregation numbers of 100%-bridged and 100%-unbridged micelles differ by only 10%; for most samples, the differences are much smaller. For the sake of simplicity, therefore, we have chosen to report aggregation numbers for block ionomers in which all divalent counterions are bridged (Table 2). Aggregation numbers for each counterion show a general increase with ionic block length, though exceptions are found for four of the metal ions at the shortest ionic block length. The diblock PS(370)-*b*-PAA(3), neutralized with Cs^+, Ba^{2+}, Cd^{2+}, and Pb^{2+}, gave anomalously large aggregation numbers, indicating the possibility of supermicellar agglomeration or nonspherical aggregate formation. Large aggregation numbers for extremely short ionic block lengths were observed previously in block ionomers containing univalent ions.[24] The four anomalous samples were omitted from all scaling analyses.

The aggregation number, Z, is related to the total volume of the micelle core by $V_{core} = ZN_Bv$, where N_B is the number of units in the insoluble block and v is the volume of a single repeat unit. The radius of a spherical ionic core can then be calculated:

$$R_{core} = \sqrt[3]{\frac{3V_{core}}{4\pi}} \qquad (4)$$

Table 3. Ionic Core Radii (Å) of Block Ionomer Micelles Containing Different Metal Ions

polymer composition PS(*x*)-*b*-PAA(*y*)	type of metal ion									
	Cs	Ba	Cd		Pb		Ni		Co	
	R_{Cs^+}	$R_{Ba^{2+}}$	$R_{Cd(Ac)^+}$	$R_{Cd^{2+}}$	$R_{Pb(Ac)^+}$	$R_{Pb^{2+}}$	$R_{Ni(Ac)^+}$	$R_{Ni^{2+}}$	$R_{Co(Ac)^+}$	$R_{Co^{2+}}$
370-*b*-3	24.9	18.6	29	25	24.3	20.7	16.4	14.0	14.5	12.4
370-*b*-7	23.0	21	23.8	20.2	20.4	17.5	23.6	20.2	23.1	19.7
370-*b*-11	29.5	26.8	33.0	28.1	29.7	25.6	34.1	29.2	29.1	24.9
370-*b*-15	36.4	30.8	33.7	28.8	31.2	27.0	39.8	34.2	37.7	32.4
370-*b*-19	40.7	36.4	38.8	33.3			48.2	41.5	46.8	40.3
370-*b*-26	47.2	46.4	52.3	45.1	43.1	37.7	54.6	47.3	55.0	47.6
730-*b*-84	84.4	80	87.0	76.0	81.4	72.4	98.0	85.6	109	95.2
300-*b*-44	74.2	93	92	81	70.8	63.6	95	83	130	115

To determine *v*, the densities of metal acrylate cores were calculated from the known value for cesium acrylate ($d = 2$ g/mL),[25] assuming that core and bulk densities were identical; considering the extremely high interfacial tension between soluble and insoluble blocks,[26] solvent-swelling in the core is very unlikely, and this assumption is believed to be valid. A more problematic question, however, is that of bridged or unbridged counterions; the volumes per repeat unit in the bridged and unbridged cases are quite different and, consequently, the core radii will also be different for a given aggregation number. Although FTIR has enabled us to make qualitative comparisons of the extent of counterion bridging for different methods of preparation, we do not consider this to be a quantitative technique; future experiments will therefore involve more precise elemental analysis of our block ionomers. For the time being, we have chosen to report two sets of ionic core radii for all samples prepared using metal acetates (Table 3): one for the case of 100%-bridged counterions, $R_{M^{2+}}$, and another for the case of 100%-unbridged counterions, $R_{M(Ac)^+}$. It should be noted that the true chemical state of the core material, and the true core radius, should lie somewhere between these extreme cases; however, given the appropriate assumptions with regard to the chemical state of the core, the "extreme" radii can be calculated to up to three significant figures, which makes them more useful quantities for the purpose of scaling analysis.

3.2. Dependence of Micellar Parameters on Insoluble and Soluble Block Lengths. Both theoretical and empirical methods have been used to determine relationships between micellar parameters and block lengths. In the theoretical approach,[27−31] expressions for the total free energy of the micelle, including terms pertaining to the core, the coronas, and the core/coronas interface, are minimized with respect to such variables as aggregation number and core radius, in order to determine the dependence of these variables on characteristics of the block copolymer. Empirical studies, on the other hand, involve the determination of micellar characteristics for several block copolymer compositions, followed by the selection of scaling laws that best fit the data.[32] We have taken the latter approach in the present study, with the additional goal of investigating the relationship between scaling laws and the metal ions in the core.

In their general form, scaling laws for the aggregation numbers and core radii of block copolymer micelles can be written

$$Z \sim N_B^{\alpha} N_A^{-\beta}$$

$$R_{core} \sim N_B^{\kappa} N_A^{-\gamma} \qquad (5)$$

This trend, where aggregation numbers and core radii increase with the insoluble block length and decrease with the soluble block length, is predicted by theory and corroborated by experimental evidence in a wide range of systems. The values of the exponents vary from system to system, depending on such factors as the chemical nature of the blocks, the type of solvent, and the relative block lengths.

We begin our analysis of scaling behavior with the six block copolymers that constitute the series PS(370)-*b*-PAA(*y*), in order to determine the scaling of aggregation numbers and ionic radii as a function of the insoluble block length (section 3.2.1). The values of the exponents and the proportionality constants are compared for different neutralizing ions. We then estimate the contribution of the soluble block length to the scaling behavior, using aggregation numbers and ionic core radii for all eight block copolymer compositions (section 3.2.2).

3.2.1. Insoluble Block Length Dependence. From the scaling relations in eq 5, we obtain the following when the length of the soluble block is a constant:

$$Z = K_Z N_B^{\alpha}$$

$$R_{core} = K_R N_B^{\kappa} \qquad (6)$$

where K_Z and K_R are proportionality constants, into which any N_A dependence has been absorbed. Taking the logarithm of these equations yields

$$\log Z = \log K_Z + \alpha \log N_B$$

$$\log R_{core} = \log K_R + \kappa \log N_B \qquad (7)$$

Plots of log Z and log R_{core} vs log N_B for a constant soluble block length are therefore linear, with slopes equal to the scaling exponents, α and κ, respectively; the proportionality constants, K_Z and K_R, are determined from the *y*-intercepts. Figure 1 shows examples of such log−log plots for block ionomer micelles in the PS(370)-*b*-PANi(*y*) series; a least-squares regression algorithm was used to determine the slopes and *y*-intercepts, along with the standard deviations on these values. Similar log−log plots were obtained for each of the other five counterions, using aggregation numbers and core radii from Tables 2 and 3, respectively.

Table 4 lists exponents and proportionality constants for the relation $Z = K_Z N_B^{\alpha}$, describing the aggregation number as a function of ionic block length for reverse micelles containing different counterions. Since all data included in this part of the analysis were obtained from samples with identical polystyrene block lengths, differences in K_Z and α could be attributed exclusively to counterion effects. The analogous relations for core radii, $R_{core} = K_R N_B^{\kappa}$, were similarly characterized for each counterion, and values of K_R and κ are listed in

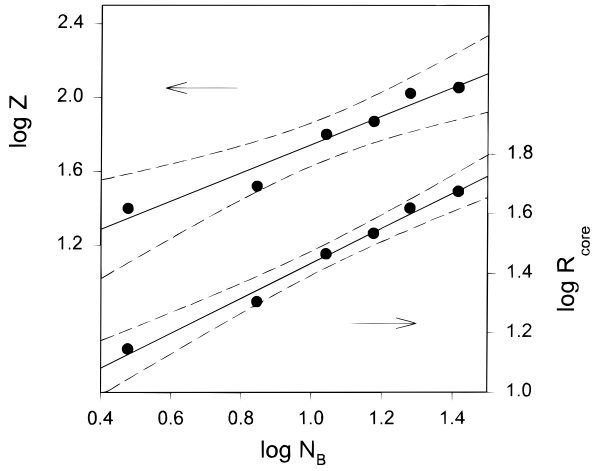

Figure 1. Plots of log aggregation number (log Z) (top) and log core radius (log R_{core}) (bottom) versus log N_B, for block ionomer micelles in the series PS(370)-*b*-PANi(y). Arrows indicate the appropriate axis for each set of data. For the relation $Z = K_Z N_B^{\alpha}$, the upper plot yields $\alpha = 0.77 \pm 0.09$ and $K_Z = 9.5 \pm 1.3$. Similarly, for $R_{core} = K_R N_B^{\kappa}$, the lower plot yields $\kappa = 0.59 \pm 0.03$, and $K_R = 7.0 \pm 1.1$ Å. The dotted lines are 99% confidence intervals.

Table 4. Ionic Block Length Dependence of Aggregation Numbers, $Z = K_Z N_B^{\alpha}$ and $Z = K_{Z,av} N_B^{0.74}$, for Micelles of PS(370)-*b*-PAA(y) Neutralized with Different Metal Ions

metal ion	r_{ion}[a] (Å)	K_Z	α	r^2 [b]	$K_{Z,av}$	r^2 [c]
Cs^+	1.67	12.0 ± 1.2	0.67 ± 0.06	0.96	9.71 ± 0.07	0.96
Ba^{2+}	1.34	8.3 ± 1.4	0.74 ± 0.13	0.92	8.36 ± 0.09	0.92
Cd^{2+}	0.97	8.9 ± 1.9	0.68 ± 0.24	0.74	7.63 ± 0.15	0.74
Pb^{2+}	1.20	6.3 ± 1.8	0.68 ± 0.22	0.84	5.27 ± 0.07	0.84
Ni^{2+}	0.69	9.5 ± 1.3	0.77 ± 0.09	0.95	10.49 ± 0.10	0.95
Co^{2+}	0.72	5.0 ± 1.3	0.89 ± 0.10	0.96	9.49 ± 0.15	0.95

[a] From: *CRC Handbook of Chemistry and Physics*, 60th ed.; CRC Press: Boca Raton, FL. [b] Correlation coefficient for linear regression of Z versus N_B^{α}. [c] Correlation coefficient for linear regression of Z versus $N_B^{0.74}$.

Table 5. Ionic Block Length Dependence of Ionic Core Radii, $R_{core} = K_R N_B^{\kappa}$ and $R_{core} = K_{R,av} N_B^{0.58}$, for Micelles of PS(370)-*b*-PAA(y) Neutralized with Different Metals Ions

counterion	K_R (Å)	κ	r^2 [a]	$K_{R,av}$ (Å)	r^2 [b]
Cs^+	7.8 ± 1.1	0.56 ± 0.02	0.99	7.33 ± 0.02	0.99
Ba^{2+}	6.5 ± 1.1	0.59 ± 0.04	0.99	6.73 ± 0.02	0.99
$Cd(Ac)^+$	8.2 ± 1.2	0.55 ± 0.08	0.94	7.54 ± 0.05	0.94
Cd^{2+}	6.8 ± 1.2	0.56 ± 0.08	0.94	6.57 ± 0.04	0.94
$Pb(Ac)^+$	7.4 ± 1.2	0.55 ± 0.08	0.97	6.67 ± 0.03	0.97
Pb^{2+}	6.1 ± 1.2	0.56 ± 0.08	0.97	5.79 ± 0.03	0.97
$Ni(Ac)^+$	8.3 ± 1.1	0.58 ± 0.03	0.99	8.37 ± 0.03	0.99
Ni^{2+}	7.0 ± 1.1	0.59 ± 0.03	0.99	7.21 ± 0.03	0.99
$Co(Ac)^+$	7.0 ± 1.1	0.63 ± 0.03	0.99	8.05 ± 0.05	0.99
Co^{2+}	5.9 ± 1.1	0.63 ± 0.03	0.99	6.93 ± 0.04	0.99

[a] Correlation coefficient for linear regression of R_{core} versus N_B^{κ}. [b] Correlation coefficient for linear regression plot of R_{core} versus $N_B^{0.58}$.

Table 5; scaling exponents and proportionality constants for both bridged and unbridged counterions are reported.

Aggregation numbers and ionic core radii for each counterion (constant soluble block length) were plotted vs N_B^{α} and N_B^{κ}, respectively, using the exponents listed in Tables 4 and 5; Figure 2 shows sample plots of Z (top) and R_{core} (bottom) for micelles of Ni^{2+} block ionomers in the series PS(370)-*b*-PANi(y). Correlation coefficients (r^2) for plots of Z vs N_B^{α} (Table 4) and R_{core} vs N_B^{κ} (Table 5) indicate excellent linear correlation for most metal ions. Ionic core radii show considerably less scatter than aggregation numbers (Table 5); five of the six metal

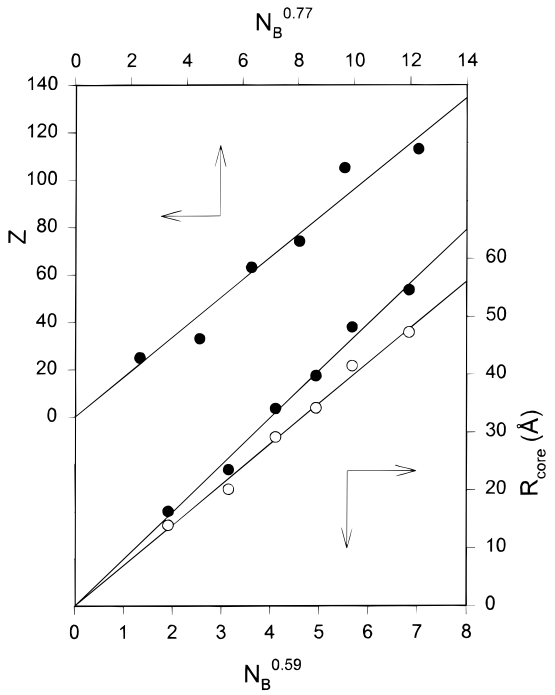

Figure 2. Plots of aggregation number (Z) versus N_B^{α} ($\alpha = 0.77$) (top) and ionic core radius (R_{core}) versus N_B^{κ} ($\kappa = 0.59$) (bottom) for micelles of PS(370)-*b*-PANi(y). Arrows indicate the appropriate axis for each set of data. For the lower plots, open circles represent the radii of cores with 100% bridged counterions, $R_{Ni^{2+}}$, and closed circles represent the radii of cores with 100% unbridged counterions, $R_{Ni(Ac)^+}$.

ions gave a linear correlation with $r^2 \geq 0.97$. With these scaling relations, therefore, it appears that the sizes of ionic cores containing a wide range of metal ions can be controlled a priori through variations in the ionic block length. For materials applications, size control within this limited range of ionic block lengths ($y = 3-26$) is extremely important, as short ionic blocks provide access to microreactors with radii <100 Å, which are best suited to nanoparticle formation.

When the scaling exponents for aggregation numbers are compared (Table 4), it is found that the differences between values of α for the six counterions are mostly within experimental error. Along with reporting the six exponents individually, therefore, we have averaged values of α to obtain $\alpha_{av} = 0.74 \pm 0.08$. Assuming an N_B dependence of $N_B^{0.74}$, aggregation numbers for different counterions were then plotted on the same ordinate scale. Sample plots of Z vs $N_B^{0.74}$ for the Ni^{2+}, Ba^{2+}, and Pb^{2+} series are shown (Figure 3, top). The slopes on the average ordinate scale, $K_{Z,av}$, were determined from regression lines forced through the origin; these values, listed in Table 4, are proportionality constants for the equation $Z = K_{Z,ave} N_B^{0.74}$. Although aggregation numbers for various counterions scale similarly with $N_B^{0.74}$, the proportionality constants are clearly dependent on the nature of the counterion. A similar strategy was applied to the ionic core radii, as the scaling exponents κ were also found to be the same for different counterions, within experimental error. An average exponent $\kappa_{av} = 0.58 \pm 0.03$ was calculated, and from linear regression of R_{core} vs $N_B^{0.58}$ (Figure 3, bottom), proportionality constants $K_{R,av}$ were determined for each counterion (Table 5). Although the scaling exponents for each counterion, α and κ, were obtained using only a small number of data points (five or six), the similarity of these values for different

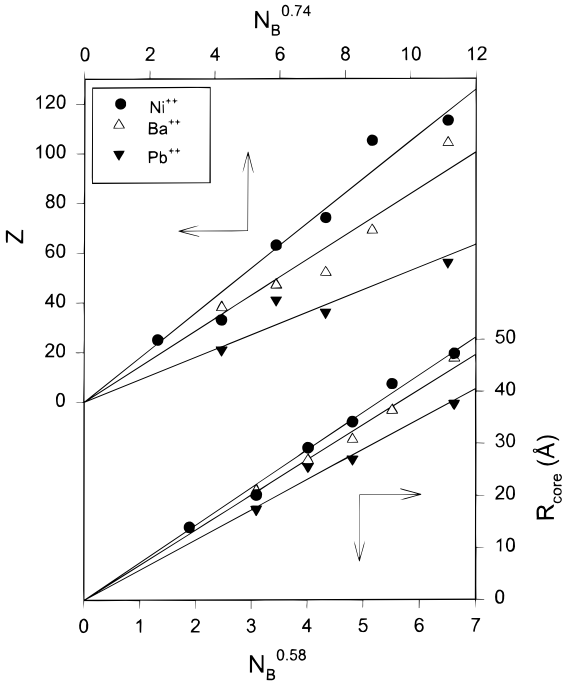

Figure 3. Plots of aggregation number (Z) versus $N_B^{0.74}$ and ionic core radius (R_{core}) versus $N_B^{0.58}$ for micelles of PS(370)-*b*-PAX(y), where X = Ni, Ba, and Pb. Arrows indicate the appropriate axes for each set of data. For the purpose of illustration, $R_{M^{2+}}$ values have been used to represent the core radii for all metal ions.

counterions suggests that the average exponents represent reliable trends within this range of ionic block lengths.

If we assume that the scaling exponents α and κ are independent of the neutralizing ion within experimental error, the effects of the counterion on Z and R_{core} are contained within the proportionality constants $K_{Z,ave}$ and $K_{R,ave}$, respectively. Values of $K_{Z,av}$, listed in Table 4, indicate that aggregation numbers of block ionomer micelles containing different counterions decrease in the following order: $Ni^{2+} > Cs^+ > Co^{2+} > Ba^{2+} > Cd^{2+} > Pb^{2+}$. It is noteworthy that Pb^{2+} and Cd^{2+} ionomers, which show the lowest fraction of micelles by SEC, also have the lowest aggregation numbers. At this point, we stress that any counterion dependence in the aggregation number is a consequence of the influence of the ion on micelle formation. This is not a trivial statement, if we consider that most ion-containing block copolymers described in the literature were prepared by the introduction of metal ions after the micelle had formed.[8−12] In the present system, however, it is the exchange between protons and counterions that initiates the self-assembly of insoluble blocks, such that metal ions play an important role in the early stages of micellization.

For the divalent metal acetates, we find a linear decrease in $K_{Z,av}$ as the crystal ionic radius (r_{ion}) of the divalent species increases (Figure 4). To explain the linear relation between micelle aggregation number and the radius of the metal ions, we consider that, as r_{ion} decreases, stronger interactions are expected between the counterions and the charged polymer units.[33] Stronger ionic interactions between (and within) poly(metal acrylate) blocks will tend to increase the surface tension of the core−solvent interface. In order to minimize this thermodynamic penalty, the system will form larger micelles as the counterions become smaller. For the Cs^+ and Ba^{2+} ionomers, prepared using metal hydroxides,

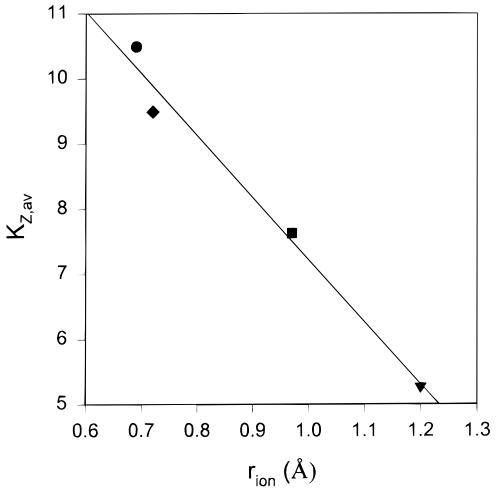

Figure 4. Plot of $K_{Z,av}$ versus the crystal ionic radius (r_{ion}) for block ionomers containing various divalent metal ions: Ni^{2+} (●), Co^{2+} (◆), Cd^{2+} (■), and Pb^{2+} (▼).

it is clear that the $K_{Z,av}$ values (9.71 and 8.36, respectively) fall significantly above the regression line, and these two series therefore do not appear to obey the trend. The unexpectedly high values of $K_{Z,av}$ for Cs^+ and Ba^{2+}, given their relatively large ionic radii (1.67 Å and 1.34 Å, respectively) may be related to the strong basicity of cesium and barium hydroxide compared with that of the metal acetates.

We now turn our attention to a brief comparison of the N_B dependence observed in the present system ($Z \sim N_B^{0.74\pm0.08}$, $R_{core} \sim N_B^{0.58\pm0.03}$) with other empirical and theoretical scaling relations. We find the scaling laws determined here to be most similar to theoretical relations for starlike micelles, $Z \sim N_B^{0.8}$, $R_{core} \sim N_B^{0.6}$.[30,31] This agrees with earlier data on the core sizes of Cs-neutralized block ionomers, which also scaled as $N_B^{0.6}$.[17] The relation determined by Zhang et al. for aqueous crewcut micelles[32] ($R_{core} \sim N_B^{0.4}$) showed a somewhat weaker N_B dependence than was determined in the present work.

It is important to note that the starting point of theoretical approaches to self-assembly is the thermodynamic equilibrium between single chains and the micellar pseudophase. As previously stated, it has been found that block ionomer micelles, in their final state, are kinetically-frozen aggregates that do not exhibit dynamic equilibrium, even under high-temperature conditions.[15] However, it is believed that rapid exchange between micelles and unimers does exist in the early stages of micellization, when the ion content of the insoluble blocks is relatively low and micelle lability is enhanced by solvent swelling.[34] As the degree of neutralization increases, solvent is expelled from the micelle and the core becomes increasingly viscous and compact. At some point, the high viscosity of the core prevents the facile movement of unimers to and from the micelle, such that the dynamic equilibrium between micelles and single chains is kinetically stalled. Although the movement of small molecules to and from the micelle cores, together with the chemical equilibria of Scheme 1, will allow further neutralization or changes in the degree of ion-bridging, the aggregate can no longer adjust to these chemical changes, and aggregation numbers are effectively frozen in. (We remind the reader that all micelles were completely neutralized in their final form, as determined by FTIR spectra.) The scaling relations observed in the frozen aggregates,

therefore, are actually "snapshots" of earlier thermodynamic states.

We have seen that Z and R_{core} scale with the insoluble block in a similar manner for all counterions, with an N_B dependence that agrees well with thermodynamically-based models of micellization. We also find that aggregation numbers and ionic core radii both show counterion dependence through their respective proportionality constants. To rationalize these observations, we point out that the factors which give rise to counterion dependence of micellar parameters (e.g., the crystal ionic radius) are not accounted for in general theories of block copolymer micelles. These "counterion factors" are unique to block ionomer systems and clearly have an influence on the overall size of the aggregates. At the same time, it appears that the power of N_B scaling is still governed by the more conventional factors of micellization (e.g., chain stretching, interfacial tension),[27−31] such that a single scaling relation can be applied equally well to a wide range block ionomers containing different metal ions.

3.2.2. Soluble Block Length Dependence. Along with the N_B dependence described above, several theoretical[27−29,31] and empirical[32] scaling laws have predicted an N_A dependence for aggregation numbers and core radii of block copolymer micelles. Although theories of starlike micelles predict that scaling with N_A is negligible, it has been found that the ionic core radii of starlike PS-*b*-PACs micelles show improved linear correlation when the length of the soluble block is considered;[32] we therefore did not to rule out the possibility of N_A dependence in the present system. Along with data obtained at constant N_A, we have also attempted to include values of Z and R_{core} for different soluble block lengths in comprehensive scaling relations for each counterion. Aggregation numbers and ionic core radii for each metal ion were plotted vs $N_B{}^{\alpha}N_A{}^{\beta}$ and $N_B{}^{\kappa}N_A{}^{\gamma}$, respectively. N_B exponents, determined previously, were held constant, while the N_A exponents, β and γ, were varied until the best linear correlation was obtained.

It was found that Z and R_{core} values for block ionomers prepared from the copolymer PS(300)-*b*-PAA(44) were unusually large, such that scaling plots could not be linearized without selecting unrealistic N_A exponents. The mole percentage of the ionic block is somewhat higher in these micelles (ca. 13%), which may account for their anomalous behavior relative to the other samples. Block ionomers of the copolymer PS(300)-*b*-PAA(44) were rejected from further scaling analysis, which left only two different soluble block lengths for our determination of scaling with N_A; the exponents β and γ are therefore considered to be very approximate values. Figure 5 shows scaling plots for the Ni^{2+} reverse micelles, including both N_A and N_B dependence.

For the complete scaling relations $Z \sim N_B{}^{\alpha}N_A{}^{-\beta}$ and $R_{core} \sim N_B{}^{\kappa}N_A{}^{-\gamma}$, N_A exponents determined for Cs^+, Ba^{2+}, Cd^{2+}, and Ni^{2+} micelles were all in the range of $\beta = 0.42 \pm 0.06$ and $\gamma = 0.14 \pm 0.02$, while Pb^{2+}- and Co^{2+}-neutralized samples showed considerably weaker scaling with the soluble block length ($\beta = 0.10 \pm 0.05$ and $\gamma = 0.04 \pm 0.02$). The observation of lower β and γ values for the last two counterions may not be physically meaningful, considering the poor statistics in our determination of N_A dependence.

3.3. DLS of Block Ionomers. 3.3.1. Basic DLS Theory. The diffusion of monodisperse, noninteracting particles in a colloidal solution results in the exponential

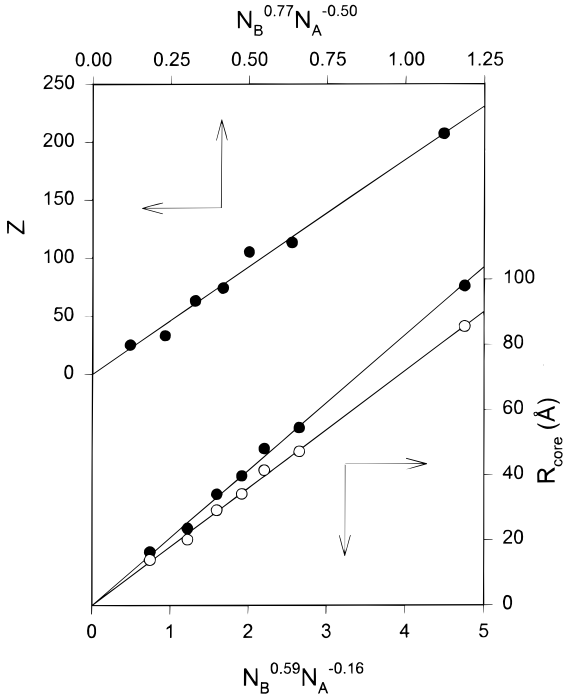

Figure 5. Plots of aggregation number (Z) versus $N_B{}^{0.77}N_A{}^{-0.50}$ (top) and ionic core radius (R_{core}) versus $N_B{}^{0.59}N_A{}^{-0.16}$ (bottom) for micelles of Ni^{2+} block ionomers. Arrows indicate the appropriate axis for each set of data.

decay of the normalized electric field autocorrelation function, $g_1(\tau)$:

$$g_1(\tau) = \exp(-\Gamma\tau) \tag{8}$$

where τ is the correlation time and Γ is the relaxation rate; Γ is related to the particle diffusion coefficient (D) by

$$\Gamma = Dq^2 \tag{9}$$

The scattering vector q is defined

$$q = (4\pi n/\lambda)\sin(\theta/2) \tag{10}$$

where n is the refractive index of the solvent, λ is the wavelength of the incident light, and θ is the angle at which scattering light is measured. The simple linear relationship between Γ and q^2 (eq 9) holds for diffusive relaxation modes and may be disrupted by interactions between particles that inhibit free diffusion.

For colloidal solutions containing a distribution of particle sizes, the resultant autocorrelation function will be made up of a distribution of relaxation rates. Detailed information on the distribution can be extracted from the autocorrelation function using sophisticated analysis techniques such as Provencher's CONTIN method.[35] For the purposes of this study, however, we have used the simpler cumulant method of Koppel,[36] which describes the total autocorrelation function as an expansion about the z-average relaxation rate, Γ_z:

$$\ln g_1(\tau) = 1 - \Gamma_z\tau + \frac{\mu}{2!}\tau^2 - \ldots \tag{11}$$

where μ is the second moment of the distribution, and the ratio $\mu/\Gamma_z{}^2$ is related to the polydispersity of the particles.

Γ_z, determined at a finite concentration of particles, is related via eq 9 to an effective z-average diffusion

coefficient, $D_{z,eff}$. In some cases, $D_{z,eff}$ will show concentration dependence in the form of the expansion

$$D_{z,eff} = D_z(1 + k_D c + ...) \quad (12)$$

The mutual *z*-average diffusion coefficient, D_z, is obtained by extrapolation to infinite dilution. The slope, k_D, of the linear extrapolation is a measure of interparticle correlations, which are a balance of direct and hydrodynamic interactions. In general, positive values of k_D arise from repulsive interactions between particles (e.g., hard sphere, electrostatic), while negative k_D values connote attractive interactions (e.g., van der Waals).

Perhaps the most fundamental parameter to describe colloidal particles is their hydrodynamic radius, R_h, which is obtained by substitution of D_z into the Stokes−Einstein relation:

$$(R_h)_z = kT/6\pi\eta D_z \quad (13)$$

where *k* is the Boltzmann constant, *T* is the temperature of the experiment, and η is the solvent viscosity at temperature *T*. As indicated in eq 13, R_h derived from cumulant analysis is a *z*-average value.

3.3.2. DLS of Selected Block Ionomers in Toluene. Several solutions of block ionomers were investigated by dynamic light scattering, in order to obtain some information on the hydrodynamic behavior of the reverse micelles. Limitations of sample availability prevented us from acquiring DLS data on all the block ionomers that were investigated by SLS; representative samples were therefore selected, covering a range of metal ions and block copolymer compositions.

Cumulant analysis of autocorrelation functions for all block ionomer micelles gave values of μ/Γ_z^2 in the range 0.05−0.20, indicating a distribution of relaxation times. It should be noted that, in some cases, low scattering intensity makes the fitting of autocorrelation functions less accurate, which often results in high values of the second cumulant; actual polydispersities may therefore be much lower than those suggested by μ/Γ_z^2. In some cases, more detailed information on colloidal polydispersities can be obtained from CONTIN analysis of the autocorrelation function; however, such an analysis was beyond the scope of the present work.

For several concentrations of micelles in toluene, values of Γ_z were plotted as a function of q^2. Figure 6a shows examples of such plots for aggregates of Cd-neutralized PS(302)-*b*-PAA(44); the linearity of Γ_z vs q^2 is indicative of free diffusion of micelles and was observed for the vast majority of reverse micelles. The concentration dependence of the slope ($D_{z,eff}$) is plotted in Figure 6b. In most cases, the diffusion coefficients of block ionomer micelles showed relatively low concentration dependence, although values of k_D were consistently negative. This suggests weak attractive interactions between the micelles in toluene, most likely of the van der Waals variety.

Table 6 lists hydrodynamic radii, R_h, calculated from D_z at infinite dilution for selected Cs^+ ionomers. The ratio R_g/R_h is also shown, as this parameter gives useful information on the micellar structure.[37] For hard spheres, R_g/R_h has a value of 0.775, while for starlike polymers, $R_g/R_h \approx 1.10$ for most aggregation numbers, and increases rapidly at low *Z*. Most of the block ionomers investigated, including those listed in Table 6, show R_g/R_h ratios between the values for hard spheres and starlike micelles, in agreement with recent results

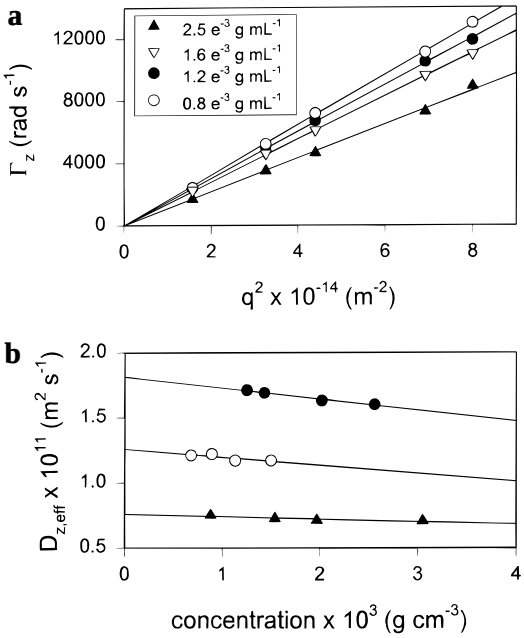

Figure 6. (a) Plots of the *z*-average relaxation rate (Γ_z) versus the square of the scattering vector (q^2) for different concentrations of micellar solutions of the block ionomer PS(300)-*b*-PACd(44). (b) Plot of the effective *z*-average diffusion coefficient ($D_{z,eff}$) versus concentration for the following block ionomers: PS(730)-*b*-PACs(84) (▲), PS(300)-*b*-PACs(44) (○), and PS(370)-*b*-PACs(15) (●).

Table 6. Structural Data for Selected Cs^+ Block Ionomer Micelles in Toluene

PS(*x*)-*b*-PACs(*y*)	*Z*	R_h (nm)	*H* (nm)	R_g (nm)	R_g/R_h
370-*b*-3	127	15	12.5	25	1.67
370-*b*-15	80	22	18.4	19	0.86
370-*b*-19	88	25	20.9	19	0.76
370-*b*-26	100	26	21.3	25	0.96
730-*b*-84	177	52	43.6	46	0.88
300-*b*-44	230	31	23.6	32	1.03

by Förster for strongly-segregated block copolymer micelles.[38] These findings are consistent with our assumption of spherical ionic cores. Structural data for block ionomers containing other metal ions are included in the Supporting Information.

Daoud and Cotton developed a scaling model for star polymers,[39] which can be applied to features of the corona in starlike block copolymer micelles. They predicted that the polymer brush height, *H*, scales as $H \sim Z^{0.2}N_A^{0.6}$ in good solvents. In the present system, *H* is the height of the corona, calculated from $H = R_h - R_{core}$, *Z* is the aggregation number of the micelle, and N_A is the number of units in the polystyrene block. For block ionomers with a constant soluble block length of PS = 370, log *H* vs log *Z* was plotted, including data for all counterions (Supporting Information), to obtain $H \sim Z^{0.3\pm0.1}$. This agrees with the theoretical scaling of brush height with aggregation number, indicating that coronal segment density profiles of block ionomer micelles are starlike, irrespective of the metal ions in the core. The N_A dependence of *H* was also estimated from a limited number of data points to obtain the full scaling relation $H \sim Z^{0.3\pm0.1}N_A^{0.9\pm0.2}$; this suggests stronger soluble block length dependence than is predicted by theory, possibly due to more extensive steric perturbations in the corona than are described by Daoud and Cotton for star polymers.

3.4. TEM of Block Ionomer Films Neutralized with Different Metal Ions. TEM micrographs of PS-

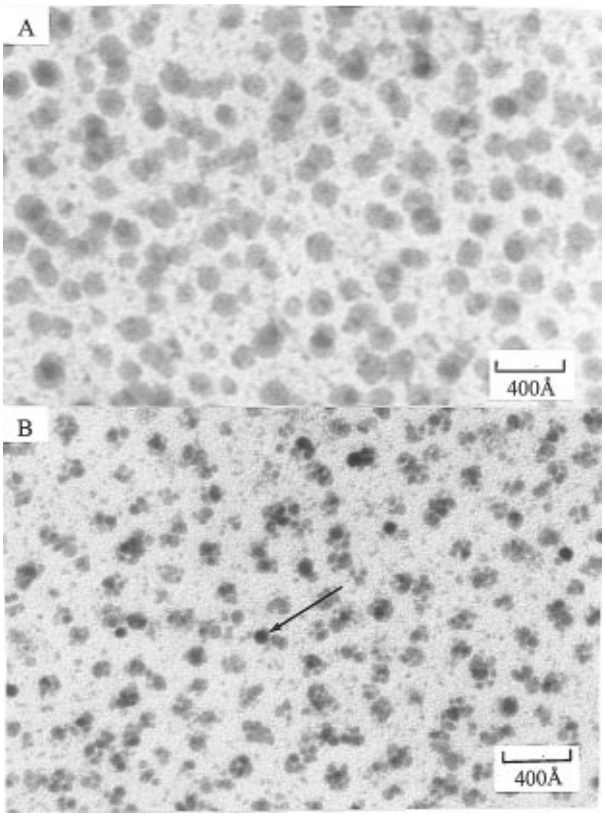

Figure 7. Transmission electron micrographs of PS(730)-*b*-PAA(84) neutralized with (A) Ba^{2+} and (B) Pb^{2+}. Dark regions indicate ionic cores dispersed in a matrix of polystyrene. The Pb^{2+}-neutralized sample (B) shows evidence of metal reduction, with some cores containing single lead particles (indicated with an arrow) of ca. 80 Å in diameter.

(703)-*b*-PAA(84) neutralized with Ba^{2+} and Pb^{2+} ions are shown in Figure 7. In both cases, the dark regions of high electron density are ion-containing microdomains dispersed in a polystyrene matrix (gray background), indicating that metal ions are localized in the micelle cores. In the Ba^{2+} block ionomer, spherical cores of low polydispersity are observed, with a radius of 80 Å, identical to R_{core} calculated from SLS data. The RPI value for the core distribution is 1.04, indicating low polydispersity. In the Cd^{2+} and Cs^{+} films (not shown), the ionic cores appeared somewhat elongated; holes and cracks in the polystyrene matrix of these films were also observed. Both elongated cores and aberrations in the matrix phase are attributable to the microtoming of these samples and may reflect differences in the mechanical properties of ionomers containing different metal ions. The elongated cores of Cd^{2+} and Cs^{+} micelles both showed distinct orientation, which is evidence that the original cores were stretched in the direction of microtoming. DLS results for the Cs^{+} sample gave $R_g/R_h = 0.88$, supporting a spherical micellar structure in solution prior to TEM sample preparation. The micrograph of Pb^{2+} reverse micelles reveals the formation of small metal particles within micelle cores, probably due to the reduction of Pb^{2+} ions within the electron beam. Close inspection of the micrograph reveals that some of the cores have formed a single lead particle (indicated with an arrow), while other cores contain clusters of smaller particles; in the latter case, the overall shape of the dark regions, while roughly spherical, is somewhat irregular. The average radius of the Pb-containing microdomains is 63 Å with an RPI of 1.02, which is about 15% lower than $R_{Pb^{2+}}$ calculated from SLS aggregation numbers. The low value of R_{core} determined from TEM can be explained by the migration of Pb "seed" particles toward the center of the core in the process of reduction and single particle formation. As well, we have measured the average radius of the single lead particles in the micrograph, which is ca. 40 Å. Assuming that the density of the particles is identical to the bulk value (11.4 g/mL), this corresponds to 9800 Pb atoms per particle. From the SLS-determined aggregation number, we have calculated that the original ionic core contains between 5200 and 10 300 Pb^{2+} ions, depending on the extent of counterion bridging. This suggests that the size of the Pb single particles is restricted by the number of Pb^{2+} ions in the cores, supporting the claim that the ionic cores can be used as true inorganic microreactors.

4. Conclusions

We have determined scaling relations for block ionomer reverse micelles of PS-*b*-PAA, in which the acid block was neutralized with a wide range of metal ions. Micelle aggregation numbers for all counterions were found to scale with the insoluble block length as $Z \sim N_B^{0.74\pm0.08}$, while ionic core radii scaled as $R_{core} \sim N_B^{0.58\pm0.03}$; both scaling relations are in agreement with theories for starlike block copolymer micelles. For most metal ions, aggregation numbers and core radii also showed significant N_A dependence, and approximate exponents were determined. Although scaling exponents, within experimental error, were independent of the counterion, aggregation numbers and core radii were found to show metal ion dependence through the proportionality constants, decreasing in the order $Ni^{2+} > Cs^{+} > Co^{2+} > Ba^{2+} > Cd^{2+} > Pb^{2+}$. For divalent counterions introduced via metal acetates, a linear relationship was found between aggregation numbers and the crystal ionic radii. R_g/R_h ratios, calculated from combined SLS and DLS data, are between the values for stars and compact spheres. The coronal brush height was found to scale as $H \sim Z^{0.3\pm0.1}N_A^{0.9\pm0.2}$.

The determination of reliable scaling laws for aggregation numbers and core radii is a critical step toward the use of block ionomer cores as inorganic micoreactors of controllable size. The present work has shown that the radii of these microreactors can be controlled, with excellent linear correlation, in the range of ca. 10 −100 Å, by variations in the length of either block or by selecting the appropriate counterion. Such control in the range of small sizes is especially important for the synthesis of metal and semiconductor nanoparticles in the ionic core; these particles of ultrasmall dimensions have interesting optical and electronic properties that can be tuned through variations in the particle size.

Reverse micelles of PS-*b*-PAA block ionomers appear to offer numerous advantages over other systems of ion-containing block copolymers, including compatibility with a large variety of counterions, facile and controllable ion addition, high stability of aggregates, and now well-characterized core sizes for a selection of different metal ions. With an understanding of scaling relations and counterion dependence, it is relatively easy to prepare inorganic microreactors of a desired size, containing a wide range of ionic precursors for small particle synthesis. We recognize the potential of a wide range of composite materials derived from block ionomers of this type, with properties that can be controlled through a priori knowledge of self-assembly in the ionomer host.

Acknowledgment. This work was supported by the Natural Sciences and Engineering Research Council of Canada (NSERC). M.M. is grateful for scholarship funding provided by NSERC and Le Fonds pour la Formation de Chercheurs et L'Aide à la Recherche (FCAR, Quebec).

Supporting Information Available: Table of f_{mic}, $M_{w,tot}$, and $M_{w,mic}$, compiled from SEC and SLS data for all block ionomers presented in this study; discussion of the effects of variations in the method of preparation on micelle parameters, including effects of the amount of added metal acetate (R) and the concentration of methanolic metal acetate solutions; a figure and table related to the preceding topic; table of structural data, including R_h, H, and R_g/R_h, for various block ionomers containing different metal ions (9 pages). Ordering information is given on any current masthead page.

References and Notes

(1) Tuzar, Z.; Kratochvil, P. *Adv. Colloid Interface Sci.* **1976**, *6*, 201.
(2) Price, C. In *Developments in Block Copolymers*; Goodman, I., Ed.; Applied Science Publishers: London, 1982; Vol. 1, p 39.
(3) Tuzar, Z.; Kratochvil, P. In *Surface and Colloid Science*; Matijevic, E., Ed.; Plenum Press: New York, 1993; Vol. 15, p 1.
(4) Selb, J.; Gallot, Y. In *Polymeric Amines and Ammonium Salts*; Goethals, E. J., Ed.; Pergamon Press: New York, 1980; p 205.
(5) Selb, J.; Gallot, Y. In *Development in Block Copolymers*; Goodman, I., Ed.; Elsevier Applied Science: London, 1985; Vol. 2, pp 27−96.
(6) Moffitt, M.; Khougaz, K.; Eisenberg, A. *Acc. Chem. Res.* **1996**, *29*, 95.
(7) Moffitt, M.; McMahon, L.; Pessel, V.; Eisenberg, A. *Chem. Mater.* **1995**, *7*, 1185.
(8) Möller, M. *Synth. Met.* **1991**, *41−43*, 1159.
(9) Cummins, C. C.; Schrock, R. R.; Cohen, R. E. *Chem. Mater.* **1992**, *4*, 27.
(10) Ng Cheong Chan, Y.; Craig, G. S. W.; Schrock, R. R.; Cohen, R. E. *Chem. Mater.* **1992**, *4*, 885. Ng Cheong Chan, Y.; Schrock, R. R.; Cohen, R. E. *J. Am. Chem. Soc.* **1992**, *114*, 7295. Yue, J.; Sankaran, V.; Cohen, R. E.; Schrock, R. R. *J. Am. Chem. Soc.* **1993**, *115*, 4409; Cohen, R. E.; Yue, J. *Supramol. Sci.* **1994**, *1*, 117.
(11) Antonietti, M.; Wenz, E.; Bronstein, L.; Seregina, M. *Adv. Mater.* **1995**, *7*, 1000.
(12) Spatz, J.; Roescher, A.; Möller, M. *Adv. Mater.* **1996**, *8*, 337.
(13) Brus, L. E. *J. Chem. Phys.* **1983**, *79*, 5566. Brus, L. E. *J. Chem. Phys.* **1984**, *80*, 4403.
(14) Henglein, A. *Chem. Rev.* **1989**, *89*, 1861.
(15) Desjardins, A.; Eisenberg, A. *Macromolecules* **1991**, *24*, 5779.
(16) Desjardins, A.; van de Ven, Th.; Eisenberg, A. *Macromolecules* **1992**, *25*, 2412.
(17) Nguyen, D.; Williams, C. E.; Eisenberg, A. *Macromolecules* **1994**, *27*, 5090.
(18) Long, T. E.; Allen, R. D.; McGrath, J. E. In *Chemical Reactions On Polymers*; Benham, J. L.; Kinstel, J. F., Eds.; ACS Symposium Series 364; American Chemical Society: Washington, DC, 1988; Chapter 19.
(19) Gauthier, S.; Duchesne, D.; Eisenberg, A. *Macromolecules* **1987**, *20*, 753.
(20) DePorter, C. D.; Ferrence, G. M.; McGrath, J. E. *Polym. Prepr. (Am. Chem. Soc., Div. Polym. Chem.)* **1993**, 574.
(21) Zimm, B. H. *J. Chem. Phys.* **1948**, *16*, 1093.
(22) Benoit, H.; Froelich, D. In *Light Scatterig from Polymer Solutions*; Huglin, M. B., Ed.; Academic Press: New York, 1972; Chapter 11.
(23) Renliang, X.; Winnik, M. A.; Hallett, F. R.; Riess, G.; Croucher, M. D. *Macromolecules* **1991**, *24*, 87.
(24) Khougaz, K.; Zhong, X. F.; Eisenberg, A. *Macromolecules* **1996**, *29*, 3937−3949.
(25) Nguyen, D. Ph.D. thesis, McGill University: Montreal, 1994.
(26) Nguyen, D.; Varshney, S. K.; Williams, C. E.; Eisenberg, A. *Macromolecules* **1994**, *27*, 5086.
(27) Whitmore, M.; Noolandi, J. *Macromolecules* **1985**, *18*, 657.
(28) Bluhm, T. L.; Whitmore, M. D. *Can. J. Chem.* **1985**, *63*, 249.
(29) Nagarajan, R.; Ganesh, K. *J. Chem. Phys.* **1989**, *90*, 5843.
(30) Halperin, A. *Macromolecules* **1987**, *20*, 2943.
(31) Zhulina, E. B.; Birshtein, T. M. *Vysokomol. Soedin.* **1985**, *27*, 511.
(32) Zhang, L.; Barlow, R. J.; Eisenberg, A. *Macromolecules* **1995**, *28*, 6055.
(33) Hird, B.; Eisenberg, A. *Macromolecules* **1992**, *25*, 6466.
(34) Khougaz, K.; Nguyen, D.; Williams, C. E.; Eisenberg, A. *Can. J. Chem.* **1995**, *73*, 2086.
(35) Provencher, S. W. *Comput. Phys. Commun.* **1982**, *27*, 213.
(36) Koppel, D. E. *J. Chem. Phys.* **1972**, *57*, 4814.
(37) Burchard, W. *Adv. Polym. Sci.* **1983**, *48*, 1.
(38) Förster, S.; Zisenis, M.; Wenz, E.; Antonietti, M. *J. Chem. Phys.* **1996**, *104*, 9956.
(39) Daoud, M.; Cotton, J. P. *J. Phys.* **1982**, *43*, 531.

MA961577X